Journal of Virology

Virology | Full-Length Text

N-terminal acetyltransferase 6 facilitates enterovirus 71 replication by regulating PI4KB expression and replication organelle biogenesis

Hang Yang,[1] Tingting Fan,[1] Meng Xun,[1] Bo Wu,[1] Shangrui Guo,[1] Xinyu Li,[1] Xiaohui Zhao,[1] Haoyan Yao,[2] Hongliang Wang[1,3]

AUTHOR AFFILIATIONS See affiliation list on p. 19.

ABSTRACT Enterovirus 71 (EV71) is one of the major pathogens causing hand, foot, and mouth disease in children under 5 years old, which can result in severe neurological complications and even death. Due to limited treatments for EV71 infection, the identification of novel host factors and elucidation of mechanisms involved will help to counter this viral infection. N-terminal acetyltransferase 6 (NAT6) was identified as an essential host factor for EV71 infection with genome-wide CRISPR/Cas9 screening. NAT6 facilitates EV71 viral replication depending on its acetyltransferase activity but has little effect on viral release. In addition, NAT6 is also required for Echovirus 7 and coxsackievirus B5 infection, suggesting it might be a pan-enterovirus host factor. We further demonstrated that NAT6 is required for Golgi integrity and viral replication organelle (RO) biogenesis. NAT6 knockout significantly inhibited phosphatidylinositol 4-kinase IIIβ (PI4KB) expression and PI4P production, both of which are key host factors for enterovirus infection and RO biogenesis. Further mechanism studies confirmed that NAT6 formed a complex with its substrate actin and one of the PI4KB recruiters—acyl-coenzyme A binding domain containing 3 (ACBD3). Through modulating actin dynamics, NAT6 maintained the integrity of the Golgi and the stability of ACBD3, thereby enhancing EV71 infection. Collectively, these results uncovered a novel mechanism of N-acetyltransferase supporting EV71 infection.

IMPORTANCE Enterovirus 71 (EV71) is an important pathogen for children under the age of five, and currently, no effective treatment is available. Elucidating the mechanism of novel host factors supporting viral infection will reveal potential antiviral targets and aid antiviral development. Here, we demonstrated that a novel N-acetyltransferase, NAT6, is an essential host factor for EV71 replication. NAT6 could promote viral replication organelle (RO) formation to enhance viral replication. The formation of enterovirus ROs requires numerous host factors, including acyl-coenzyme A binding domain containing 3 (ACBD3) and phosphatidylinositol 4-kinase IIIβ (PI4KB). NAT6 could stabilize the PI4KB recruiter, ACBD3, by inhibiting the autophagy degradation pathway. This study provides a fresh insight into the relationship between N-acetyltransferase and viral infection.

KEYWORDS enteroviruses, acetyltransferase, Golgi morphology, replication organelle, ACBD3

Enterovirus is a genus of virus that belongs to the family of *Picornaviridae*, which could cause a variety of diseases, including non-specific febrile illness, hand, foot, and mouth disease (HFMD), encephalitis, and respiratory diseases (1). Among these viruses, enterovirus 71 (EV71) has recently caused large outbreaks of HFMD in Southeast Asia with several hundred deaths reported (2). Therefore, EV71 is a big threat to children, especially those under 5 years old.

Editor Mark T. Heise, University of North Carolina at Chapel Hill, Chapel Hill, North Carolina, USA

Address correspondence to Hongliang Wang, hongliangwang@xjtu.edu.cn.

The authors declare no conflict of interest.

See the funding table on p. 19.

Received 6 November 2023
Accepted 7 December 2023
Published 8 January 2024

Enteroviruses spread mainly through fecal-oral route and initiate infection by targeting host cells in the primary sites of replication in the gastrointestinal tract (1, 3). As a non-enveloped virus, EV71 binds to cell surface receptors, including scavenger receptor B2 (SCARB2) with its capsid, and enters host cells via endocytosis (4, 5). The low pH in the endosome leads to uncoating and cytosol release of viral genome, which is a positive-sense, single-stranded RNA of ~7,400 nucleotides long (1). The genome of EV71 encodes a large polyprotein that would be processed into four structural proteins: VP1–VP4 and seven nonstructural (NS) proteins: 2A, 2B, 2C, 3A, 3B, 3C, and 3D (6, 7). The four structural proteins assemble to form icosahedral viral particles with a diameter of about 20–30 nm, while the NS proteins are essential for viral polyprotein processing and viral replication (6, 7). Recent studies have also revealed an upstream open reading frame in certain enteroviruses, which encodes a small protein to promote viral growth in gut epithelial cells (8, 9).

Like other positive-sense RNA viruses, replication of enteroviruses occurs on specialized membrane structures that are remodeled from host intracellular membrane replication organelles (ROs) (10–12). The ROs of enteroviruses are usually described as clusters of membrane structures occupying large areas of the perinuclear cytoplasm, and they are believed to have originated from the endoplasmic reticulum (ER) and *trans*-Golgi network (13, 14). In addition, the morphology of enterovirus ROs develops and changes during the course of viral infection with single-membrane structures in the earlier stages of infection, which will be transformed into double-membrane vesicles and multiple membrane structures as the infection progresses (14, 15). Genome replication by the RNA-dependent RNA polymerase (3D) generates double-stranded RNA (dsRNA) intermediates, which will ultimately lead to the production of large quantities of newly synthesized genomic RNA. Viral particles are assembled with genomic RNA and capsid proteins and then released outside of cells via lytic or non-lytic pathways (1).

The formation of ROs and efficient replication of enteroviruses require a specific set of host factors, among which phosphatidylinositol 4-kinase IIIβ (PI4KB) is one of the critical host factors (16). PI4KB primarily localizes to the Golgi apparatus, and it is a key lipid kinase that regulates Golgi-derived vesicle transport (17). During enterovirus infection, viral 3A protein was shown to modulate GBF1/Arf1 to enhance recruitment of PI4KB to ROs, where it catalyzes the production of PI4P lipids from PI, and PI4P lipids could then promote viral RNA (vRNA) synthesis or recruit lipid transfer protein—OSBP (16, 18, 19). Later, PI4KB was shown to be recruited to Golgi and viral ROs via another Golgi protein, acyl-coenzyme A binding domain containing 3 (ACBD3) (20, 21). This PI4KB recruitment also generated specialized membrane structures that are enriched in PI4P to facilitate viral replication (20). However, unlike GBF1/Arf1-mediated recruitment, this recruitment of PI4KB to the ROs was not affected by brefeldin A.

In addition to PI4KB, numerous other host factors that are required for enterovirus infection have been identified with genome-wide CRISPR/Cas9 or haploid genetic screening (22–25). In a previous study, we identified several N-terminal acetyltransferases (NATs), which are candidate host factors for EV71 infection (24). NAT is a newly characterized family of enzymes with emerging functions that contribute to human health, development, and disease (26). N-terminal acetyltransferase 8 has been shown to promote EV71 infection by increasing the stability of viral NS proteins (24). The functions of other NATs during viral infection are not well understood.

Here, in this study, we confirmed that N-terminal acetyltransferase 6 (NAT6) is an essential host factor for EV71 infection, and inhibition of NAT6 led to a drastic reduction in EV71 infection. Further studies revealed that NAT6 promoted EV71 replication by enhancing ROs biogenesis, while it has little effect on viral release. Mechanism study demonstrated that NAT6 could enhance ACBD3 stability and maintain Golgi integrity through modulating its substrate-actin, thereby promoting EV71 infection.

RESULTS

NAT6 is a key host factor for EV71 infection

To explore whether NAT6 is involved in EV71 infection, we employed the CRISPR/Cas9 gene editing system using sgRNAs targeting NAT6. SK-N-SH cells stably transduced with lentiviral vectors encoding the sgRNA were first validated for gene targeting with immunoblotting. Figure 1A shows that either sgRNA could inhibit NAT6 expression or sgRNA2 could completely inhibit NAT6 expression. Correlated to NAT6 expression, viral VP1 expression was also reduced significantly and completely abolished in the sgRNA2-transduced cells (Fig. 1A). In consonance with this, vRNA quantification (Fig. 1B) also showed reduction correlated to the degree of NAT6 inhibition. We then assessed the effect of NAT6 depletion on virus production. Figure 1C shows that the average viral titer was $10^{7.19}$ $TCID_{50}$/mL in control cells, while the NAT6 sgRNA1 and sgRNA2 cells showed $10^{6.58}$ $TCID_{50}$/mL and $10^{5.89}$ $TCID_{50}$/mL, respectively. Furthermore, EV71 infection could cause a striking cytopathic effect (CPE) in host cells, and we found that NAT6 inhibition could significantly reduce the CPE caused by viral infection as measured by cell viability (Fig. 1D), also suggesting that NAT6 is essential for EV71 infection. As NAT6 sgRNA2 inhibited NAT6 expression and EV71 infection more prominently, we next mainly used sgRNA2-transduced cells for the following experiments and referred to these cells as NAT6 knockout (KO) cells.

In order to confirm the specificity of this sgRNA-mediated knockout, sgRNA-resistant NAT6 cDNA was introduced to NAT6 KO cells to rescue NAT6 expression (Fig. 1E). Exogenous expression of NAT6 rescued viral VP1 expression (Fig. 1E) and vRNA replication (Fig. 1F), further confirming that NAT6 is essential for EV71 infection.

To test whether NAT6 could support viral infection of other enterovirus strains, control or NAT6 KO cells were infected with Echovirus 7 (Echo7) or coxsackievirus B5 (CVB5), both of which are close members in the family of *Picornaviridae*. Similar to EV71, neither Echo7 (Fig. 1G) nor CVB5 (Fig. 1H) could infect the NAT6 KO cells, suggesting NAT6 might be a pan-enterovirus host factor.

Next, we wanted to know whether NAT6 expression was affected by viral infection. To this end, SK-N-SH cells were infected with EV71, and NAT6 expression was assayed at the protein or mRNA level. Figure 1I and J shows that NAT6 expression remained unchanged with EV71 infection. Taken together, the above results suggest that NAT6 is an important host factor for enterovirus infection.

NAT6 is relevant to EV71 replication

To find out at which specific stage NAT6 functions, we infected control or NAT6 KO cells with EV71 and viral titers were monitored at various time points. Compared to control cells, reduced viral titers were observed starting 8 h post-infection (h.p.i.) as revealed by the one-step virus growth curve (Fig. 2A). Similarly, by using a full-length, infectious virus with a NanoLuc reporter (27), we found a significant reduction of luciferase at 8 or 12 h.p.i (Fig. 2B). These results together suggest that NAT6 functions at a later stage of viral infection (viral replication, virus assembly, or virus release). To confirm this, we first tested whether NAT6 could influence EV71 attachment or internalization. By measuring the vRNA with q-RT-PCR, we first showed that depletion of SCARB2, the receptor of EV71, significantly inhibited EV71 virus attachment or internalization. In contrast, comparable amounts of viruses were found to attach to or internalize control or NAT6 KO cells (Fig. 2C and D). These results suggest that NAT6 does not affect EV71 viral entry.

We next employed an EV71 subgenomic replicon (SGR) reporter, in which part of the structural gene was replaced with *Renilla* luciferase and thereby could not generate new progeny virions (27). We transfected SGR RNA into control or NAT6 KO cells, and Fig. 2E shows that, compared to control cells, luciferase began to decrease at 4 h post-transfection (h.p.t) in NAT6 KO cells, and by 8 or 12 h.p.t, a drastic decrease was observed. A polymerase dead mutant of EV71 SGR (SGR-GND) was also tested and a comparable but

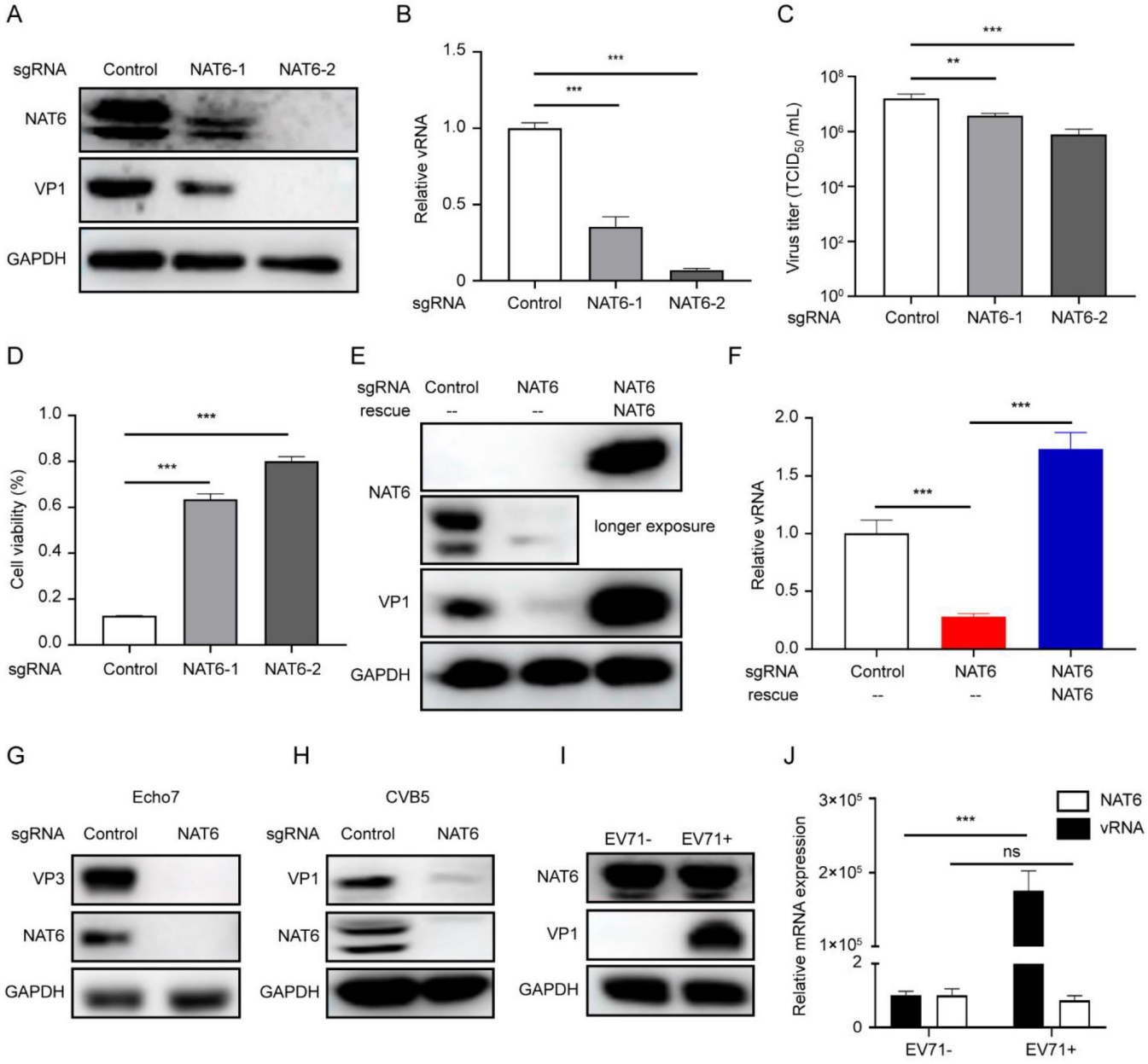

FIG 1 NAT6 is a host factor for EV71 infection in SK-N-SH cells. (A) SK-N-SH cells stably transduced with control or NAT6 sgRNA were infected with the EV71 virus (MOI = 5). After 24 h, cells were immunoblotted with NAT6 or EV71 VP1 antibody. GAPDH was used as a loading control. (B) vRNA from cells as described in panel A was quantified with q-RT-PCR. Values are normalized to control. ***$P < 0.001$. (C) Progeny viruses from the above cells were titrated. **$P < 0.01$ and ***$P < 0.001$. (D) Cells as described above were infected with EV71, and cell viability was determined at 24 h post-infection. Values are normalized to uninfected control cells. ***$P < 0.001$. (E) Control or NAT6 KO SK-N-SH cells were transduced with Flag-tagged sgRNA-resistant NAT6 and then infected with EV71. After 24 h, cells were immunoblotted with NAT6 or EV71 VP1 antibody. GAPDH was used as a loading control. (F) Cells as described in panel E were infected with EV71, and vRNA was quantified with q-RT-PCR. Values are normalized to control. ***$P < 0.001$. (G and H) SK-N-SH cells stably transduced with control or NAT6 sgRNA were infected with Echo7 virus (G, MOI = 5) or CVB5 virus (H, MOI = 1) for 24 h. Cells were then immunoblotted with Echo VP3 or CVB VP1 antibody. GAPDH was used as a loading control. (I and J) SK-N-SH cells were either mock infected or infected with EV71 (MOI = 5) for 24 h, and NAT6 or viral VP1 expression was determined by immunoblotting (I) or q-RT-PCR (J).

reduced reading was obtained (Fig. 2E). These results suggest that NAT6 is essential for EV71 replication.

Based on these observations, we hypothesized that NAT6 might be associated with viral ROs. Immunostaining showed that NAT6 displayed a diffused cytosolic distribution

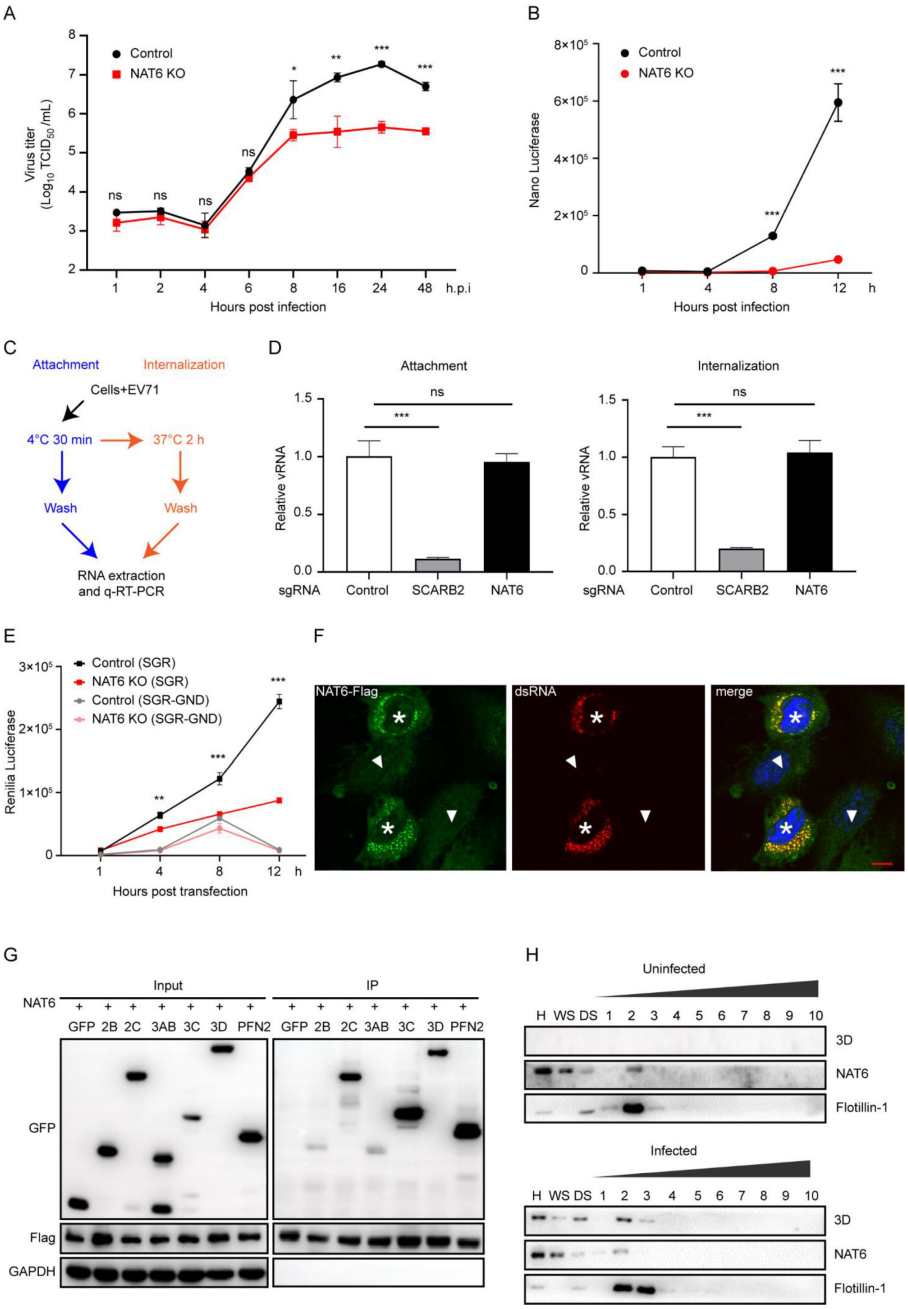

FIG 2 NAT6 is relevant to EV71 replication. (A and B) Control or NAT6 KO SK-N-SH cells were infected with EV71 (A) or EV71 with NanoLuc reporter (B), and viral titer (A) or luciferase activity (B) was determined at indicated time points. ns, not significant. *P < 0.05; **P < 0.01; and ***P < 0.001. (C) Schematic diagram of virus attachment and internalization assay. (D) Control, NAT6 KO, or SCARB2 KO SK-N-SH cells were treated with EV71 (MOI = 10) as described in panel C. Attached (left panel) or internalized (right panel) vRNA was quantified with q-RT-PCR. Values are normalized to control. ns, not significant. (E) Control or NAT6 KO SK-N-SH cells were transfected with EV71 SGR or EV71 SGR-GND RNA. Luciferase activity was determined at indicated time points. **P < 0.01 and ***P < 0.001. (F) SK-N-SH cells stably expressing NAT6-Flag were infected with EV71 (MOI = 5) for 24 h. Cells were then fixed and stained with antibodies against Flag (green) and dsRNA (red) with DAPI nuclear counterstaining (blue). Asterisk indicates infected cell, and arrowhead indicates uninfected cell. Bar, 10 µm. (G) 293T cells cotransfected with NAT6-Flag and green fluorescent protein (GFP)-tagged 2B, 2C, 3AB, 3C, 3D, or PFN2 plasmids were immunoprecipitated with anti-Flag antibody, and interactions between NAT6 and viral NS proteins were detected by anti-GFP antibody. (H) Uninfected or EV71-infected SK-N-SH cell homogenates (H) were centrifuged to prepare a "water-soluble" supernatant (WS) or "detergent-soluble" (DS) fraction. Detergent-resistant membranes were then fractionated on a density gradient. Fractions (numbered in order from light to heavy) were analyzed by immunoblotting for the indicated proteins.

(Fig. 2F, arrowheads), which is consistent with a previous report (28). In contrast, part of the NAT6 colocalized with the intermediate of viral RNA genome replication (dsRNA) after EV71 infection (Fig. 2F, asterisks), suggesting NAT6 either directly interacts with or is in close proximity to viral ROs. Enterovirus ROs are remodeled by viral NS proteins from host intracellular membranes (12). To test whether there are direct interactions between NAT6 and viral NS proteins, 293T cells were cotransfected with a plasmid expressing NAT6-Flag and a plasmid expressing green fluorescent protein (GFP)-tagged NS protein 2B, 2C, 3AB, 3C, or 3D. Profilin 2 (PFN2), which has been shown to interact with NAT6 (29), was included as a positive control. Figure 2G shows that 2C, 3C, 3D, and PFN2 co-immunoprecipitated with NAT6, while 2B and 3AB showed weak interaction, suggesting NAT6 could directly interact with viral NS proteins.

The ROs of enterovirus are enriched in cholesterol, which is crucial for optimal enterovirus replication (30, 31). These cholesterol-rich microdomains are resistant to cold detergent extraction and exhibit low buoyant densities on gradient centrifugation (19, 32). A membrane flotation assay of detergent-resistant membranes (DRMs) in EV71-infected cells showed that NAT6 cofractionated with 3D protein as well as the DRM marker flotillin-1 (Fig. 2H). Taken together, all these results suggest that NAT6 localizes to EV71 replication organelles to promote viral replication.

NAT6 is required for Golgi apparatus integrity in SK-N-SH cells

NAT6 is a member of the N-terminal acetyltransferase family and could transfer the acetyl group from acetyl-CoA to the N-terminal alpha-amino group of a protein (26). To test whether the acetyltransferase activity of NAT6 is required for viral infection, we made a catalytic-dead mutant of NAT6 (W105F, R170Q, G173D, and Y205F) (28). We then tested whether the complementation of this mutant in NAT6 KO cells could rescue EV71 infection. Our results showed that while this mutant was expressed at a high level, it failed to support EV71 infection (Fig. 3A and B), suggesting that the catalytic activity of NAT6 is required to support EV71 infection.

A previous report showed that NAT6 is essential for the structural integrity of the Golgi apparatus, and NAT6 KO caused Golgi fragmentation in the near-haploid cell line HAP1 cells (33). To evaluate the effect of NAT6 KO in SK-N-SH cells, we first checked the expression of the *cis*-Golgi marker GM130 or the *trans*-Golgi marker TGN46. We found that the expression of both proteins was unchanged in NAT6 KO cells (Fig. 3C and D, upper left panels). Next, we checked the subcellular distribution of these proteins. In control cells, both Golgi markers are typically located at the perinuclear area, indicative of Golgi localization. In contrast, fragmented staining patterns were observed for both markers in NAT6 KO cells (Fig. 3C and D, right panels). Statistical analysis showed that a significantly higher number of NAT6 KO cells displayed fragmented distribution of GM130 or TGN46 (Fig. 3C and D, lower left panels). These results suggest that NAT6 is also required for Golgi apparatus integrity in SK-N-SH cells.

NAT6 is not required for EV71 viral release

The fact that NAT6 KO caused Golgi fragmentation prompted us to speculate that the vesicular transport or protein secretion is compromised in NAT6 KO cells. Indeed, β-COP staining also showed fragmented distribution (Fig. 4A), suggesting the vesicular transport is affected. To test the efficiency of protein secretion, we measured the luciferase activity of a secreted NanoLuc in the supernatant of cell cultures. Compared to control cells, NAT6 KO cells showed significantly reduced protein secretion (Fig. 4B).

Enteroviruses have been reported to leave cells utilizing the secretory autophagy pathway (34, 35). We next wanted to know whether NAT6 also plays a role in the EV71 virus release. For this purpose, viral particles from cell culture supernatants (extracellular) or from infected cells (intracellular) were harvested to infect naive cells, and then vRNA was quantified with q-RT-PCR while viral titers were measured by $TCID_{50}$ (Fig. 4C). Figure 4D shows that both intracellular and extracellular viral RNA had a comparable degree of inhibition in NAT6 KO cells compared to control cells, suggesting viral release was not

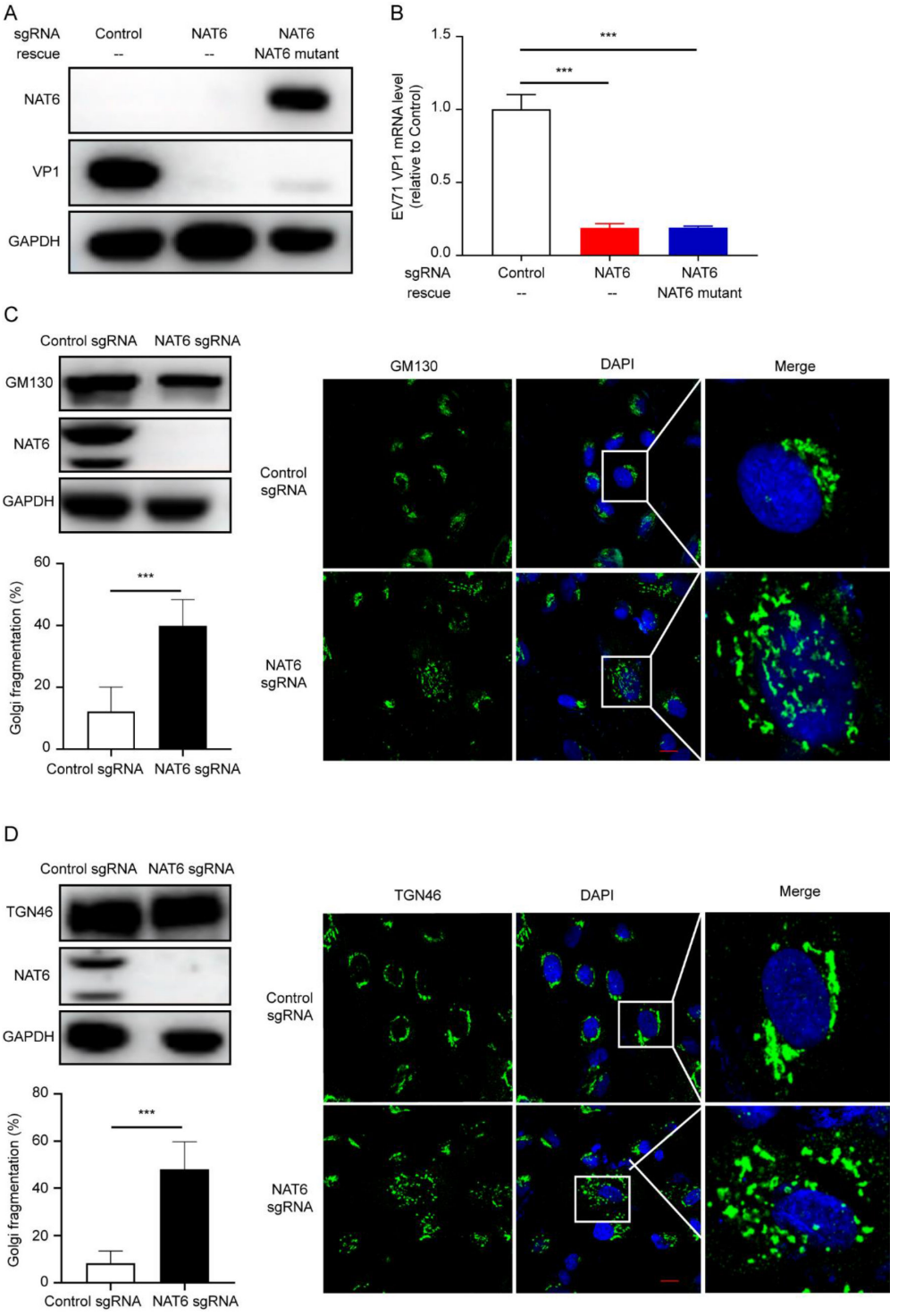

FIG 3 NAT6 is essential for Golgi integrity in SK-N-SH cells. (A and B) Control or NAT6 KO SK-N-SH cells were transduced with sgRNA-resistant catalytic-dead NAT6 mutant and then infected with EV71. After 24 h, viral VP1 expression was determined by immunoblotting (A) or q-RT-PCR (B). (C) Upper left: control or NAT6 KO SK-N-SH cells were immunoblotted with NAT6 or GM130 antibody. GAPDH was used as a loading control. Right panel: control or NAT6 KO SK-N-SH cells were immunostained with antibodies against GM130. Bar, 20 µm. Percentage of cells with fragmented Golgi was quantified and shown in the lower left panel. ***$P < 0.001$. (D) Upper left: control or NAT6 KO SK-N-SH cells were immunoblotted with NAT6 or TGN46 antibody. GAPDH was used as a loading control. Right panel: control or NAT6 KO SK-N-SH cells were immunostained with antibodies against TGN46. Bar, 20 µm. Percentage of cells with fragmented Golgi was quantified and shown in the lower left panel. ***$P <$ 0.001.

affected. Similarly, viral titration showed that both intracellular and extracellular viral particles had more than 75% reduction in NAT6 KO cells compared to control cells. Combined with viral infection and SGR results (Fig. 1 and 2), these results suggest that NAT6 is primarily required for viral replication and does not specifically regulate virus release.

NAT6 is required for the biogenesis of replication organelles

The replication organelles of enteroviruses have been reported to originate from ER and *trans*-Golgi networks (12, 13). Since the Golgi apparatus is fragmented in NAT6 KO cells, we speculated that viral replication organelles might be affected. As viral mRNA translation is coupled to RNA replication in most positive-sense viruses, a replication-independent expression system is often employed to study viral replication organelle biogenesis (36, 37). Here, we designed a replication-independent system driven by T7 promoter, followed by an EMCV IRES and EV71 NS protein-encoding region [pTM1 (2A–3D), Fig. 5A]. Control or NAT6 KO cells stably expressing the T7 polymerase

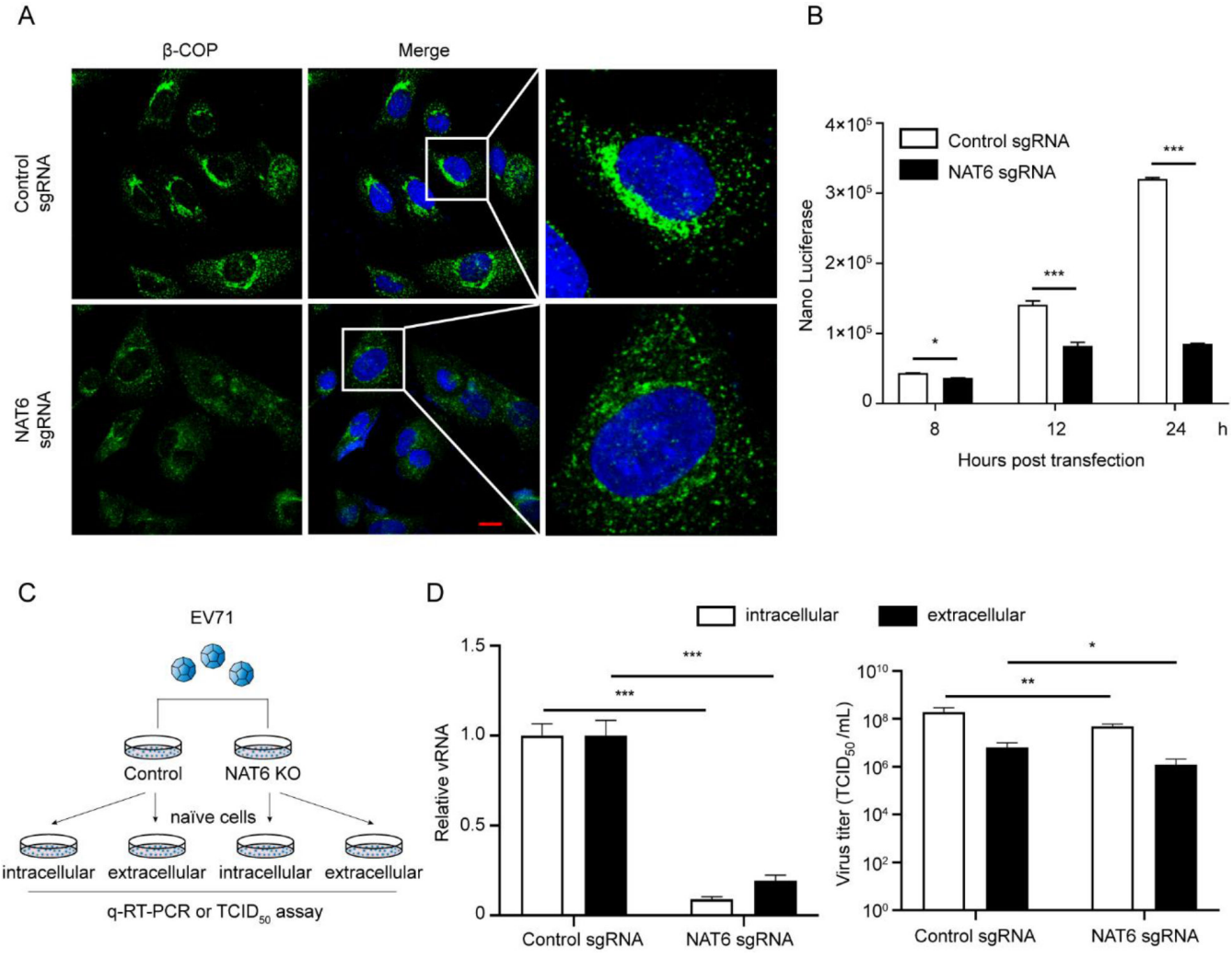

FIG 4 NAT6 is dispensable for EV71 viral release. (A) Control or NAT6 KO SK-N-SH cells were immunostained with β-COP (green) and counterstained with DAPI (blue). Bar, 10 µm. (B) Control or NAT6 KO SK-N-SH cells were transfected with a plasmid encoding secreted NanoLuc, and luciferase from the supernatant was determined at indicated time points. *P < 0.05 and ***P < 0.001. (C) Schematic diagram of EV71 reinfection assay. Extracellular viruses from the supernatant and intracellular viruses from freeze-thawed cell lysate were used to inoculate naive SK-N-SH cells for vRNA quantitation or naive RD cells for viral titration. (D) Left panel: extracellular or intracellular vRNA was determined by q-RT-PCR, and values were normalized to control cells. ***P < 0.001. Right panel: extracellular or intracellular viral titers were determined and expressed as $TCID_{50}$/mL. *P < 0.05 and **P < 0.01.

transfected with this construct led to comparable polyprotein expression, as revealed by 3D immunoblotting (Fig. 5B), suggesting this system could circumvent the flaws with replication systems and could enable RO biogenesis mechanistic studies independent from vRNA replication.

During viral infection, enteroviruses induce cytosolic vesicle clusters that comprise single-membrane, double-membrane, or multi-membrane structures (14, 15). To assess the function of NAT6 in RO biogenesis, we then examined the membrane alterations in the above T7-driven polyprotein expression system with transmission electron microscopy. Membrane alterations with clusters of vesicles could be easily observed in the perinuclear cytoplasm in control cells with packed membrane structures (Fig. 5C, upper panels). In contrast, dramatic membrane alterations were barely observed in NAT6 KO cells, and only a few trafficking vesicles were observed (Fig. 5C, lower panels). Quantification analysis of these vesicles showed that the number of vesicles was significantly reduced in the NAT6 KO cells, while the diameters of vesicles were comparable between these two groups of cells (Fig. 5D), suggesting that NAT6 is required for EV71 RO biogenesis.

NAT6 regulates PI4KB and ACBD3 expression

PI4KB, a critical host factor for enterovirus infection and RO formation, is primarily localized to the Golgi complex (38). Here, we found that PI4KB also showed fragmented distribution in NAT6 KO cells (Fig. 6A), suggesting its function might also be affected. More importantly, PI4KB was found to be significantly downregulated in NAT6 KO cells (Fig. 6B). This might explain why RO biogenesis was significantly inhibited in NAT6 KO cells. Furthermore, as the primary role of PI4KB is to catalyze the production of PI4P, we also compared the Golgi PI4P expression (39) in control and NAT6 KO cells. As expected, PI4P was also significantly reduced in NAT6 KO cells due to decreased PI4KB expression (Fig. 6C and D).

However, PI4KB mRNA was not downregulated (Fig. 6E), suggesting the reduction of PI4KB is likely to occur on a protein level. PI4KB has been shown to be recruited to the viral replication sites via the GBF1/Arf1 pathway or ACBD3 pathway during picornavirus infection (16, 40). We then examined the expression of Arf1 or ACBD3 and found that ACBD3 but not Arf1 was downregulated in NAT6 KO cells (Fig. 6F and G). Further analysis also confirmed that the downregulation of ACBD3 was not caused by transcriptional inhibition (Fig. 6H). These results together suggest that NAT6 might maintain PI4KB expression through the ACBD3 pathway in SK-N-SH cells.

NAT6 stabilizes ACBD3 by inhibiting autophagy-lysosome degradation

To find out the connections between NAT6 and ACBD3, we first tested whether there is an interaction between NAT6 and ACBD3 by co-immunoprecipitation (Co-IP). In SK-N-SH cells stably expressing NAT6, NAT6 co-immunoprecipitated with endogenous ACBD3 (Fig. 7A). Similarly, in SK-N-SH cells stably expressing ACBD3, we found that ACBD3 could also co-immunoprecipitate with endogenous NAT6 (Fig. 7B), suggesting there is an interaction between NAT6 and ACBD3.

ACBD3 comprises several distinct domains, including an N-terminal Acyl-CoA binding domain (ACBD), a coiled-coil domain (CC) in the middle, and a Golgi dynamics domain (GOLD) at the C-terminus (41). We then generated three ACBD3 mutants, each lacking one of the above domains: ΔACBD, ΔCC, and ΔGOLD (Fig. 7C). We found that ΔACBD and ΔCC could still interact with NAT6, while ΔGOLD could not (Fig. 7D), suggesting ACBD3 interacts with NAT6 through its GOLD domain.

NAT6 KO leads to decreased ACBD3 expression (Fig. 6G). Next, we wanted to know how NAT6 overexpression affects the expression of ACBD3. For this purpose, 293T cells were co-transfected with a fixed amount of ACBD3 together with an increasing amount of NAT6. Immunoblotting showed that NAT6 overexpression upregulated ACBD3 expression in a dose-dependent manner (Fig. 7E), suggesting NAT6 is essential to

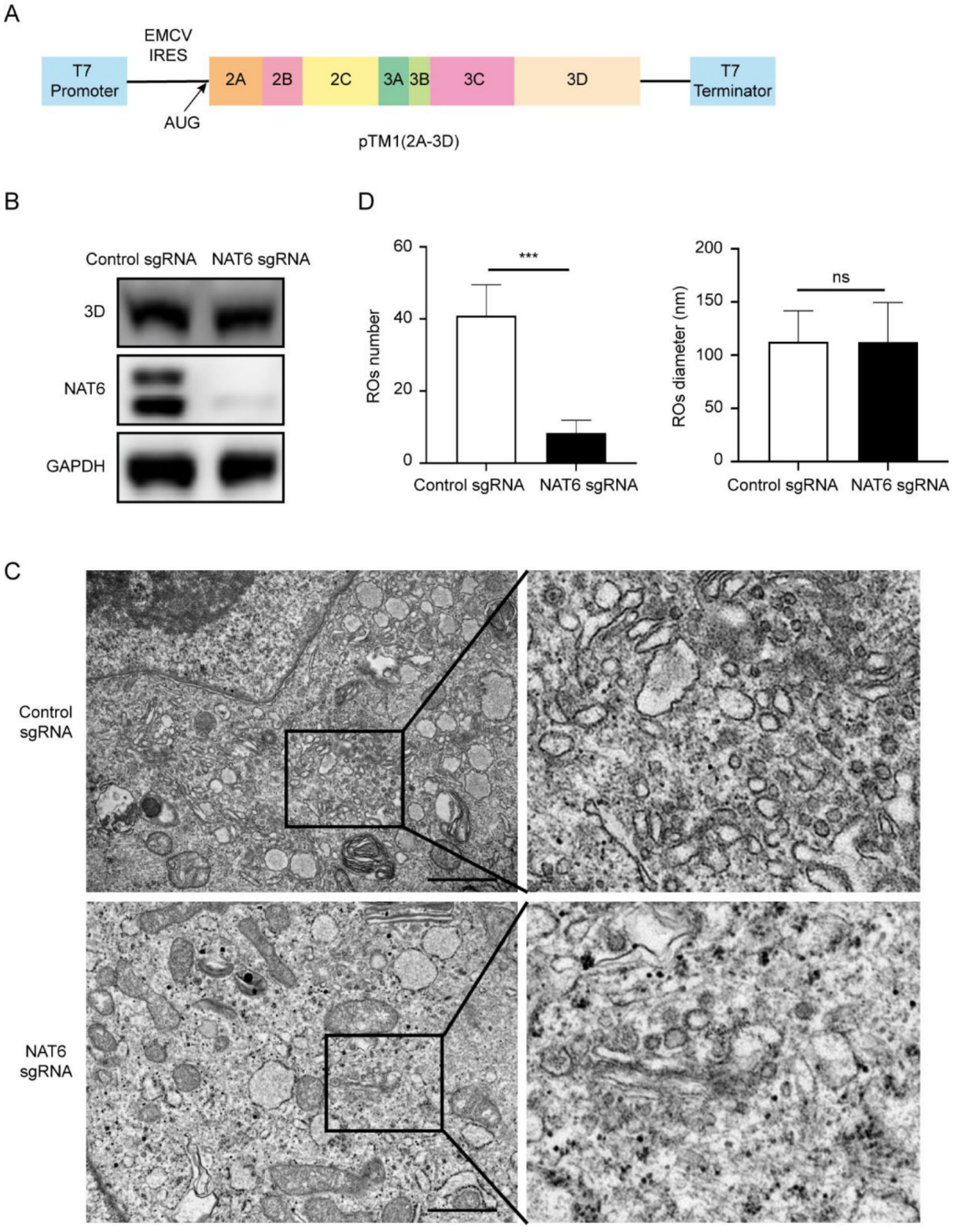

FIG 5 NAT6 supports viral RO biogenesis. (A) Schematic diagram of pTM1 (2A–3D). The EV71 NS encoding region was inserted into the pTM1 backbone under the control of a T7 promoter and EMCV IRES, followed by a T7 terminator. (B) Control or NAT6 KO cells stably expressing T7 RNA polymerase were transfected with pTM1 (2A–3D), and expression of viral 3D protein was determined 36 h post-transfection with immunoblotting. (C) Control or NAT6 KO cells as described in panel B were prepared for transmission electron microscope. Enlargements of the boxed areas are shown in the right panels. Bar, 1 µm. (D) Quantification of the number and diameter of vesicles in panel C. ns, not significant. ***$P < 0.001$.

maintain ACBD3 expression in cells. Our previous study has shown that another N-acetyltransferase, NAT8, upregulated EV71 NS proteins by increasing their stability (24).

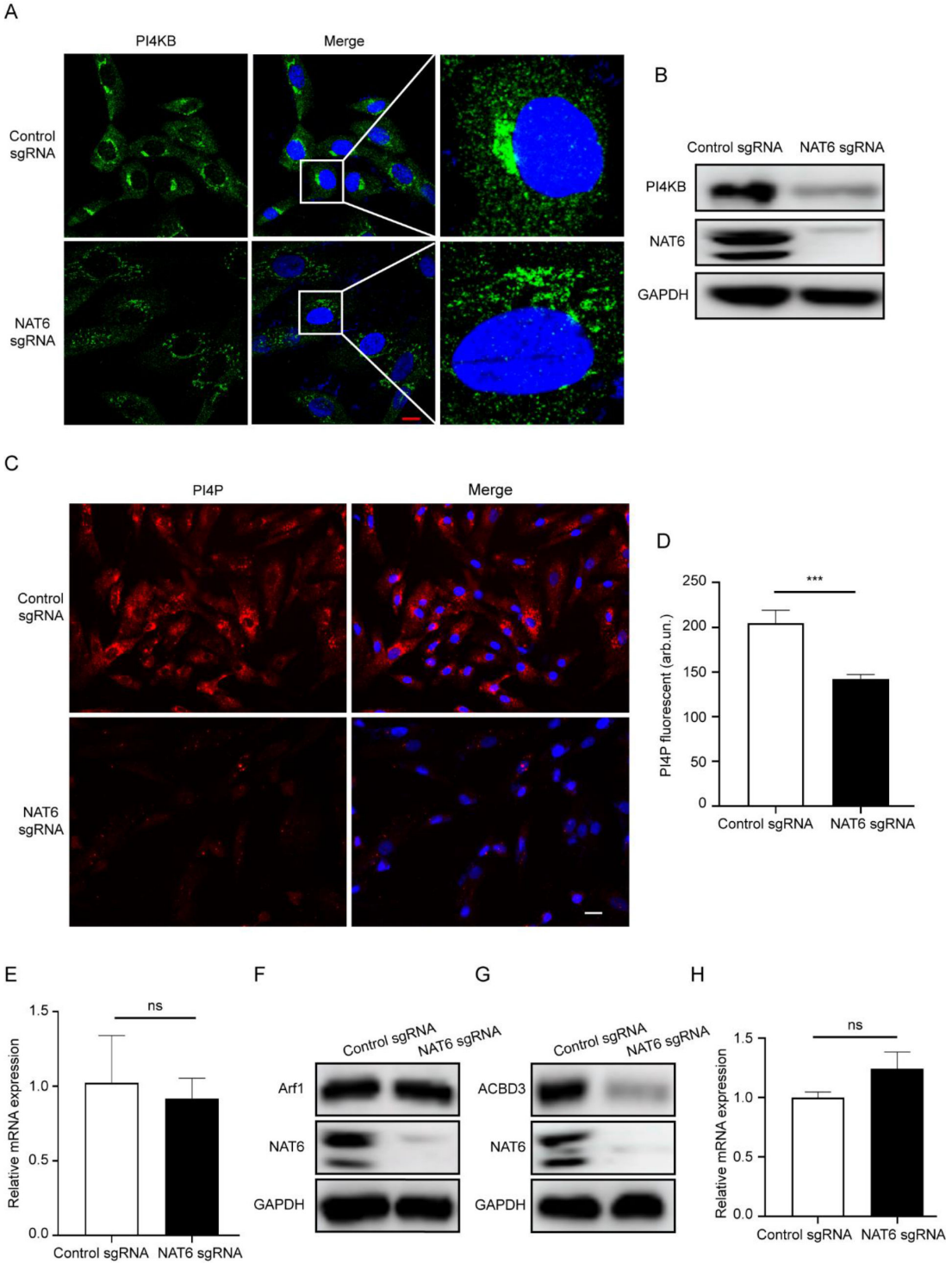

FIG 6 NAT6 regulates PI4KB and ACBD3 expression. (A) Control or NAT6 KO SK-N-SH cells were immunostained with PI4KB (green) and counterstained with DAPI (blue). Bar, 10 µm. (B) Control or NAT6 KO SK-N-SH cells were immunoblotted with indicated antibodies. (C) Control or NAT6 KO SK-N-SH cells were immunostained with an antibody against PI4P (red) and counterstained with DAPI (blue). Bar, 20 µm. (D) Quantitation of PI4P fluorescence from control or NAT6 KO SK-N-SH cells. ***$P < 0.001$. (E) PI4KB mRNA expression from control or NAT6 KO SK-N-SH cells was determined with q-RT-PCR. ns, not significant. (F and G) Control or NAT6 KO SK-N-SH cells were immunoblotted with Arf1 (F) or ACBD3 (G) antibody. (H) ACBD3 mRNA expression from control or NAT6 KO SK-N-SH cells was determined with q-RT-PCR.

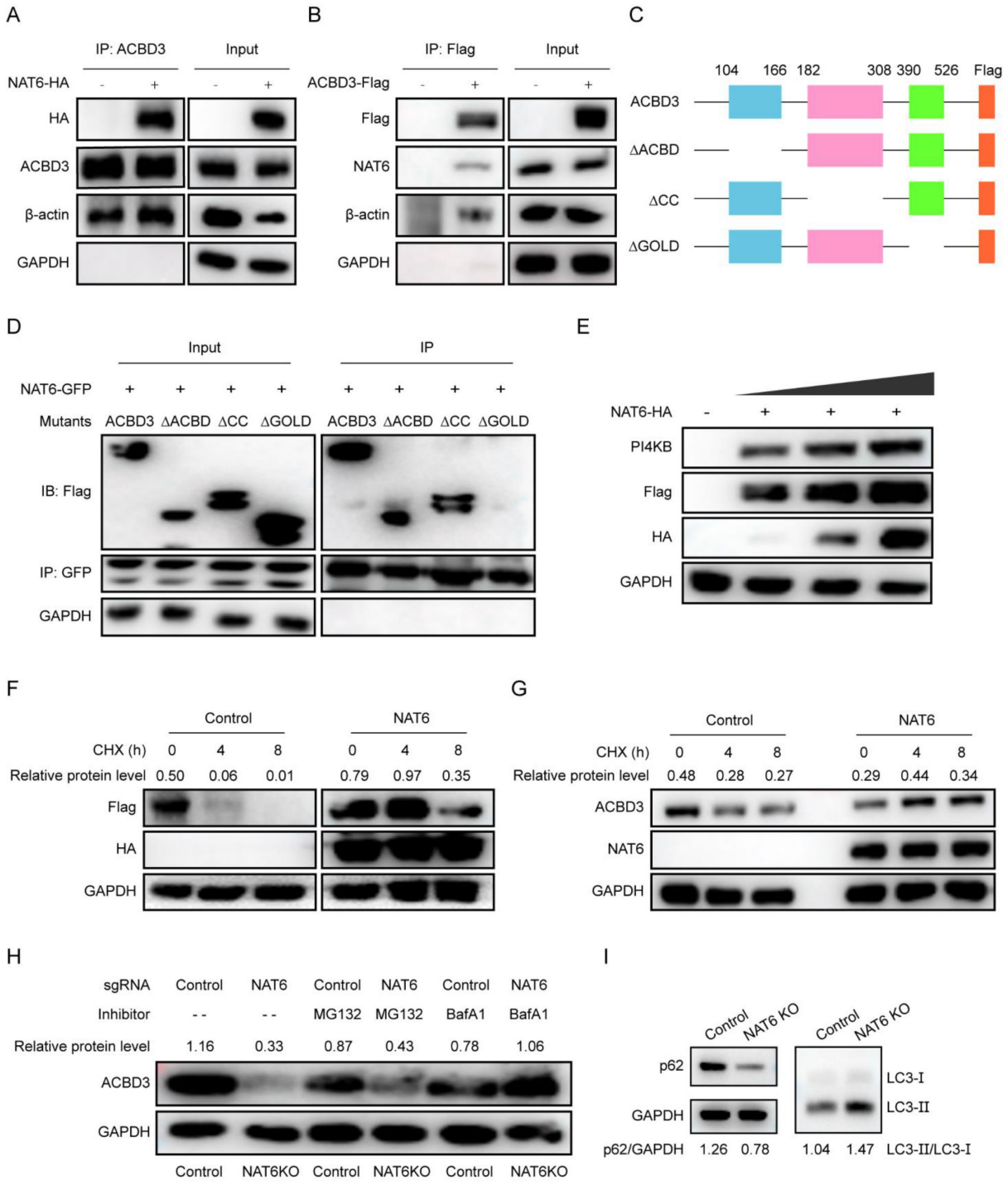

FIG 7 NAT6 interacts with ACBD3 and actin and stabilizes ACBD3 by suppressing the autophagy-lysosome degradation pathway. (A) SK-N-SH cells stably expressing NAT6-HA were immunoprecipitated using anti-ACBD3 antibody and immunoblotted with antibodies against ACBD3 or β-actin. (B) SK-N-SH cells stably expressing ACBD3-Flag were immunoprecipitated using anti-Flag antibodies and immunoblotted with antibodies against NAT6 or β-actin. (C) Schematic diagram of human ACBD3 domains and truncations. The amino acid residues are indicated on top. (D) HEK293T cells cotransfected with NAT6-GFP and ACBD3-Flag or truncated ACBD3-Flag were immunoprecipitated using anti-GFP antibody, and interactions between NAT6 and ACBD3 or mutants were detected with immunoblotting. (E) HEK293T cells cotransfected with a fixed amount of ACBD3-Flag, PI4KB, and an increasing amount of NAT6-HA plasmid (300, 600, and 900 ng) for 24 h before they were immunoblotted with indicated antibodies. (F) Mock or NAT6-HA were cotransfected with ACBD3-Flag into HEK293T cells for 18 h before they were treated with protein synthesis inhibitor cycloheximide (CHX) (100 μM). Cell lysates were collected at indicated time points and immunoblotted with indicated antibodies. The relative ACBD3 band density was normalized to that of GAPDH and shown on top. (G) SK-N-SH cells stably

(Continued on next page)

FIG 7 (Continued)

expressing NAT6-HA were treated with CHX (125 µM). Cell lysates were collected at indicated time points and immunoblotted with indicated antibodies. The relative ACBD3 band density was normalized to that of GAPDH and shown on top. (H) Control or NAT6 KO SK-N-SH cells were treated with DMSO, MG132 (10 µM), or bafilomycin A1 (BafA1) (10 nM) for 24 h. Cell lysates were collected at indicated time points and immunoblotted with indicated antibodies. The relative ACBD3 band density was normalized to that of GAPDH and shown on top. (I) Control or NAT6 KO SK-N-SH cells were immunoblotted with anti-LC3 and p62 antibodies. The relative amount of p62/GAPDH and LC3-II/LC3-I was shown below.

Since NAT6 could also upregulate ACBD3 expression in cells, we speculated that it might enhance its stability. To test this possibility, the amount of ACBD3 was determined in the presence of protein synthesis inhibitor cycloheximide (CHX) with or without NAT6 co-expression. In control cells, the amount of ACBD3 decreased significantly during CHX treatment (Fig. 7F, left panel). In contrast, in the presence of NAT6, ACBD3 maintained a similar amount after 4 h of CHX treatment and only decreased slightly by 8 h (Fig. 7F, right panel). Similar results were obtained when SK-N-SH cells stably expressing NAT6 were treated with CHX and endogenous ACBD3 was measured (Fig. 7G). All these results suggest that NAT6 could enhance the stability of ACBD3 protein in cells.

Ubiquitin-proteasome and autophagy-lysosome systems are two major intracellular protein degradation pathways in eukaryotes. Proteins degraded by proteasome could be blocked by MG132 treatment, while autophagy-mediated protein degradation can be blocked by bafilomycin A1 (BafA1). To test which pathway was involved in ACBD3 degradation during NAT6 inhibition, the amounts of ACBD3 were measured in the presence of MG132 or BafA1. Figure 7H shows that BafA1 could block the protein degradation in NAT6 KO cells, while MG132 could not, suggesting that NAT6 stabilizes ACBD3 through inhibiting autophagy-lysosome-dependent degradation. In consonance with this, the LC3-II expression was upregulated in NAT6 KO cells, while the long-lived protein p62, which is degraded by autophagy, was decreased (Fig. 7I). These results suggest that autophagy was activated in NAT6 KO cells.

NAT6 supports Golgi integrity and EV71 infection by regulating actin dynamics

Actin is the only known substrate of NAT6, and knockout of NAT6 affects actin dynamics, leading to increased cell motility and cell protrusion formation (42). Indeed, phalloidin staining revealed that filamentous actin (F-actin) signals were higher in the NAT6 KO SK-N-SH cells (Fig. 8A). We then speculated that altered actin dynamics disrupted Golgi integrity and ACBD3 expression in the NAT6 KO cells. Consistent with this hypothesis, we found that β-actin was co-immunoprecipitated along with NAT6 and ACDB3, while the cytosolic protein GAPDH was not (Fig. 7A and B). It is widely accepted that the cytoskeleton could regulate Golgi architecture, and both the actin-depolymerizing agent and the actin-stabilizing agent could lead to Golgi morphology changes (43, 44), suggesting normal actin dynamic is required to maintain Golgi integrity. To evaluate the roles of actin on Golgi integrity and EV71 infection, we treated SK-N-SH cells with jasplakinolide (Jpk). Jpk is a filamentous actin stabilizer, which increases the ratio of F-actin to actin monomer, a phenomenon similar to that observed in NAT6 KO cells (42, 45). As expected, Jpk treatment led to enhanced F-actin staining (200 nM) and an even higher concentration of Jpk treatment (500 nM) caused actin aggregates (Fig. 8B), as previously reported (46). In addition, Jpk treatment also disrupted Golgi staining, causing Golgi fragmentation (Fig. 8C). More importantly, Jpk also inhibited EV71 infection at the dose that disrupts Golgi and actin integrity (Fig. 8D), suggesting actin dynamic is required to maintain EV71 infection.

To find out the possible links between NAT6/actin and Golgi integrity, we did another Co-IP and found Golgi reassembly and stacking protein 55 (GRASP55) was also co-immunoprecipitated along with ACBD3 and NAT6, but TGN46, GM130, and GRASP65 were not (Fig. 8E). GRASP55 is a Golgi stacking protein that could tether adjacent Golgi membranes into stacks and ribbons by forming homodimers, during which actin is also required (47). Therefore, these results suggest that NAT6 and actin might regulate Golgi

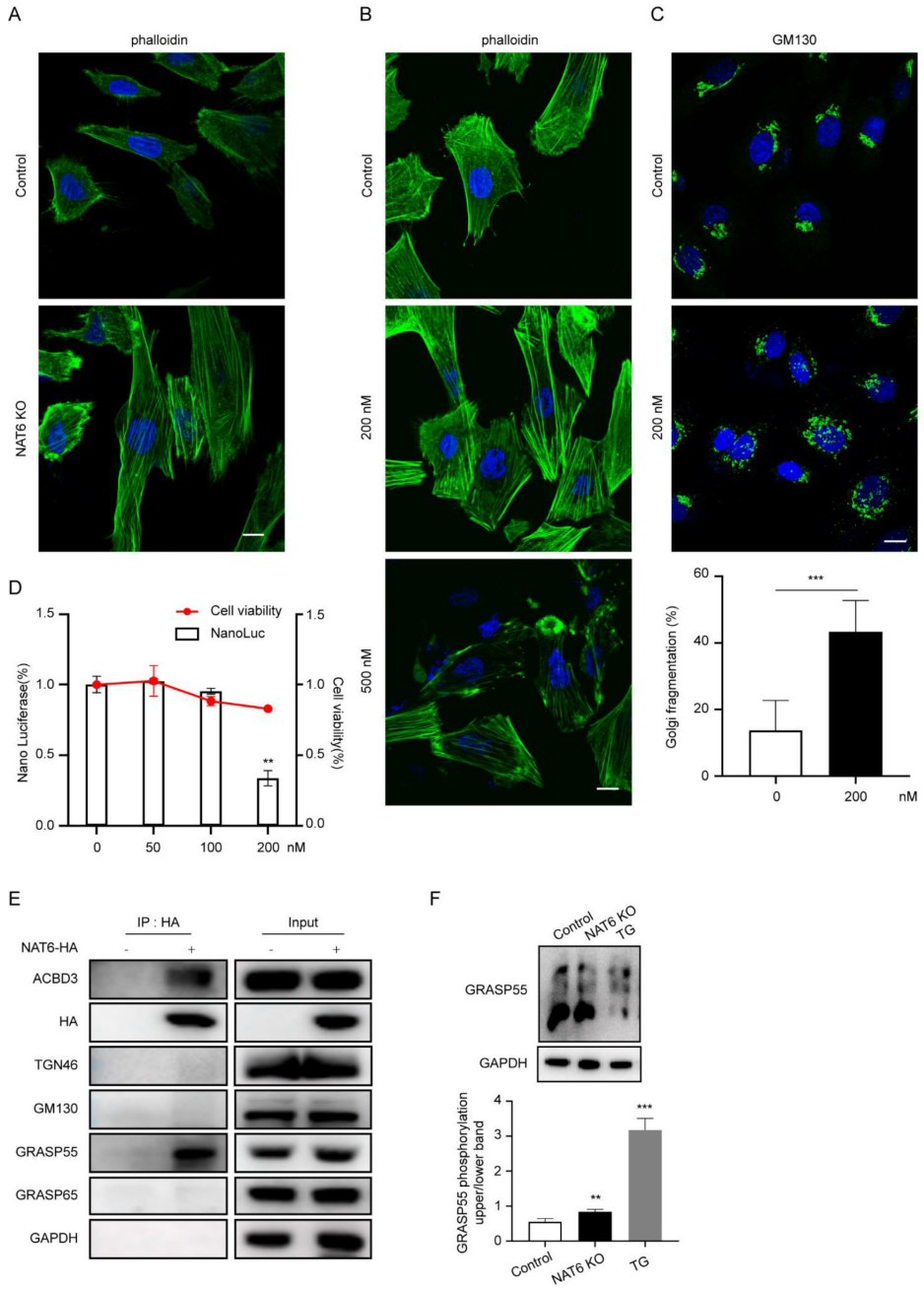

FIG 8 NAT6 supports Golgi integrity and EV71 infection by regulating actin dynamics. (A) Control or NAT6 KO SK-N-SH cells were stained with FITC-phalloidin (green) and counterstained with DAPI (blue). Bar, 10 µm. (B) SK-N-SH cells were treated with 200 or 500 nM Jpk for 1 h and then stained with FITC-phalloidin with nuclei counterstained with DAPI. Bar, 10 µm. (C) SK-N-SH cells were treated with 200 nM Jpk for 1 h and then stained with anti-GM130 with nuclei counterstained with DAPI. The percentage of cells with fragmented Golgi was quantified and shown below. Bar, 10 µm. (D) SK-N-SH cells infected with EV71-NanoLuc were treated with indicated amounts of Jpk for 12 h, and luciferase activity was determined. Cellular ATP content was determined to assess cytotoxicity. $^{**}P < 0.01$. (E) SK-N-SH cells stably expressing NAT6-HA were immunoprecipitated with anti-HA antibodies and immunoblotted with the indicated antibodies. (F) Control or NAT6 KO SK-N-SH cells were analyzed by Phos-tag gel and immunoblotted with anti-GRASP55 antibody. Thapsigargin (TG) treatment was used as a positive control of phospho-GRASP55 induction.

integrity through GRASP55. While GRASP55 oligomerization is necessary for Golgi tethering, phosphorylation of this protein will lead to membrane unlinking and unstacking. Here, we found that GRASP55 phosphorylation was upregulated in NAT6 KO cells

(Fig. 8F), suggesting its role of Golgi membrane tethering is compromised due to actin dynamic failure in NAT6 KO cells.

DISCUSSION

N-terminal acetylation, the transfer of acetyl group from acetyl-coenzyme A to the N terminus of a substrate protein, is a protein modification that has been overlooked for a long time. In fact, it is estimated that about 80% of human proteins are modified by different types of NATs (26). N-terminal acetylation affects proteins in different ways; for example, it might affect the protein half-life, the protein subcellular localization, or protein-protein interactions (26). The roles of NATs during viral infection have not been well understood. We previously showed that NAT8, an ER-localized NAT, promoted EV71 infection by stabilizing viral NS proteins (24). Here, we showed that another NAT, NAT6, facilitates EV71 infection by maintaining Golgi integrity and promoting viral RO biogenesis.

The NS proteins of enteroviruses have been reported to alter ER or *trans*-Golgi networks as a site of replication, where a negative-strand copy of RNA is first synthesized, which will serve as a template to synthesize a large quantity of new positive RNAs (1). Here, we showed that NAT6 KO cells showed fragmented Golgi morphology. As the origin of enterovirus ROs, disruption of Golgi integrity also led to reduced viral RO formation and viral replication.

Many proteins and lipids participate in the biogenesis of ROs and replication of viral genomes, among which PI4KB is a well-studied host factor (16). Recruitment of PI4KB in the ROs generates a PI4P-enriched microenvironment that enhances 3D polymerase to initiate genomic replication (16). PI4P could also recruit downstream effector proteins, like OSBP to further enhance viral replication (18, 19). PI4KB recruitment to viral ROs has been reported to be mediated by GBF/Arf1 or ACBD3 (16, 21, 40, 48). Here, we showed that in NAT6 KO cells, PI4KB and ACBD3 expression was significantly downregulated while Arf1 was not, suggesting NAT6 could regulate PI4KB expression through maintaining ACBD3 expression. Indeed, we found NAT6 overexpression upregulated ACBD3 expression by enhancing its stability.

NAT6 has been described as a highly selective NAT, with actin as its substrate (28, 49). NAT6 selectively acetylated the negatively charged N terminus of actin (26, 49). Here, we showed that β-actin was co-immunoprecipitated with NAT6 and ACBD3, together with Golgi stacking protein GRASP55. ACBD3 has been proven to be a scaffold protein to form complex with several Golgi proteins, such as GRASP55 and PI4KB (50, 51). Taken together, these results suggested that NAT6, actin, ACBD3, and GRASP55 could form a complex to maintain the normal morphology and function of the Golgi complex.

It has been previously shown that Golgi stacking protein could recruit the actin elongation factor Mena to the Golgi membrane, which will promote local actin polymerization and GRASP oligomerization, leading to Golgi ribbon linking (52). On the other hand, disruption of actin dynamics with either cytochalasin D or Jpk altered Golgi morphology, exhibiting either swollen or fragmented Golgi stacks (44). Here, we showed that GRASP55 phosphorylation was upregulated in NAT6 KO cells, which will lead to the disassembly of GRASP oligomers and subsequent Golgi ribbon unlinking and unstacking (47). Furthermore, we showed that Jpk treatment altered Golgi staining and inhibited EV71 infection in SK-N-SH cells, resembling the phenotype observed in NAT6 KO cells. Taken together, these results suggest that actin dynamic mis-regulation in NAT6 KO cells inhibits GRASP55 function, which ultimately leads to Golgi fragmentation and EV71 infection inhibition.

Actin polymerization has also been reported to be necessary for the initiation and maturation of autophagosomes as well as for the fusion of autophagosome-lysosome (53). NAT6 KO stabilizes and increases the amount of F-actin, which will potentially enhance cellular autophagy. Consistent with this theory, here we found that NAT6 KO cells showed increased LC3-II expression and p62 degradation, suggesting autophagy is activated. When cells were treated with autophagy inhibitor-BafA1, they showed an

increased amount of ACBD3. Therefore, these results suggest that NAT6 maintains ACBD3 expression and EV71 infection by inhibiting the overactivation of autophagy. On the other hand, controversial data have been reported regarding the impacts of autophagy on EV71 infection, with most of the studies revealing positive roles (54). Therefore, EV71 might manipulate autophagy in multiple ways, and the specific influence of different stages of autophagy on the EV71 replication cycle remains to be investigated.

MATERIALS AND METHODS

Cell lines, viruses, and reagents

All cells were maintained at 37°C in a 5% CO_2 humidified incubator. HEK 293T, human rhabdomyosarcoma (RD) cells, and human neuroblastoma SK-N-SH cells were obtained from the American Type Culture Collection. HEK 293T and RD cells were cultured in Dulbecco's Modified Eagle Medium (Gibco, USA) supplemented with 10% (vol/vol) fetal bovine serum (FBS; OPCELL), 100 U/mL penicillin, and 1 µg/mL streptomycin (Beyotime Biotechnology, China). SK-N-SH cells were cultured in the minimal essential medium (Hyclone) containing 10% (vol/vol) FBS. The EV71 virus and CVB5 virus have been previously described (27, 55). Echo7 virus was obtained from Xi'an Municipal CDC, propagated and expanded in RD cells, and titrated on RD cells.

The following antibodies were used in this study: rabbit-anti-NAT6, rabbit-anti-EV71 VP1, and rabbit-anti-CVB5 VP1 were from GeneTex (Taiwan, China). Mouse-anti-GAPDH, rabbit-anti-TGN46, rabbit-anti-Arf1, and rabbit-anti-PI4KB were purchased from ProteinTech (Rosemont, IL, USA). Rabbit-anti-GFP, rabbit-anti-flag, and rabbit-anti-β-actin were from ZenBio (Chengdu, China). Rabbit-anti-EV71 3D, rabbit-anti-flotillin-1, rabbit-anti-ACBD3, rabbit-anti-GM130, rabbit-anti-LC3B, rabbit anti-p62, rabbit-anti-GRASP55, and rabbit-anti-GRASP65 were from Abclonal (Woburn, MA, USA). Mouse-anti-HA and mouse-anti-Flag were from Origene (Rockville, MD, USA). Rabbit-anti-dsRNA (9D5) was purchased from Absolute Antibody (UK). Mouse-anti-β-COP was from Santa Cruz (Dallas, TX, USA). Mouse-anti-PI4KB for immunostaining was from BD Biosciences (Franklin Lakes, NJ, USA). The mouse-anti-PI4P IgM antibody was from Echelon Biosciences (Salt Lake City, UT, USA). Mouse-anti-pan EV, HRP-conjugated secondary antibodies, and Alexa Fluor 488- or 555- conjugated secondary antibodies were from Thermo Fisher Scientific.

The following reagents were used in this study: FITC-Phalloidin was purchased from Beyotime (Shanghai, China). DAPI (4',6-diamidino-2-phenylindole) was purchased from Thermo Fisher Scientific. Cycloheximide, MG132, and Bafilomycin A1 were purchased from MedChemExpress (Monmouth Junction, NJ, USA). Jasplakinolide was purchased from Abcam (Cambridge, UK). Phosbind acrylamide was purchased from ApexBio (Boston, MA, USA).

NAT6, ACBD3, PI4KB, and viral NS protein expression constructs

The coding sequences of NAT6, ACBD3, and PI4KB were amplified with a cDNA library prepared from 293T cells and subcloned into a lentiviral expression vector (56) with an appropriate tag by standard molecular cloning techniques. Where applicable, silent mutations were introduced into NAT6 genes to render them resistant to sgRNA targeting. The catalytic dead mutant of NAT6 was constructed with Gibson Assembly to introduce the following mutations: W105F, R170Q, G173D, and Y205F. The coding regions of ACBD3 truncations or mutants are indicated in Fig. 7C. Viral NS plasmids have been previously described (24). For the non-replicative EV71 polyprotein expression system, the coding region of 2A–3D and the 3′ untranslated region (UTR) of EV71 were subcloned into pTM1 backbone to drive polyprotein expression with T7 promoter and encephalomyocarditis virus (ECMV)-derived internal ribosome entry site (IRES). All constructs were confirmed by sequencing. Primer sequences were available upon request.

Lentiviral vector preparation and transduction

VSV-G pseudotyped lentiviruses were produced as previously reported (19, 57). sgRNA sequences used in this study were as follows: sgNAT6-1: GAGGAGACCCCAGCTCCTAG ; sgNAT6-2: GGAGCCTGTGCACCGCCGAC; and sgSCARB2: TGTAGACCAGAGTATCGAGA. SK-N-SH cells were transduced with lentiviral particles prepared above, and stable cell lines were obtained by puromycin selection (for sgRNA) or blasticidin S selection (for overexpression constructs). SK-N-SH cells stably expressing T7 polymerase were obtained with 600 µg/mL G418 selection.

Virus titration

Control or NAT6 KO cells were infected with EV71 at MOI = 5 for 24 h. Cell supernatants were harvested for extracellular virus titration. Intracellular virus was harvested with three cycles of freeze and thaw, followed by centrifugation to remove cell debris. For the one-step growth kinetic curve, cells were infected with EV71 at MOI = 1, and both intracellular and extracellular viruses were harvested at indicated time points as described above and pooled for titration. Virus titration was carried out with RD cells, and CPE was observed to calculate 50% tissue culture infective dose ($TCID_{50}$) with the Reed-Muench method.

Luminescence assay

Full-length EV71 reporter viruses, subgenomic EV71 replicon, and polymerase dead mutant version of EV71 SGR (SGR-GND) were described previously (27). Nano luciferase and *Renilla* luciferase were measured with the Nano-Glo or *Renilla* luciferase assay system from Promega. Cell viability assays were carried out using the Cell Titer-Glo Luminescent Cell Viability Assay Kit (Promega, Madison, WI, USA) following the manufacturer's instructions. Luminescence signals were measured using the BioTek Neo2 microplate reader.

Virus attachment and internalization assay

Viral binding and internalization assays were performed as previously described (24). Briefly, control or NAT6 KO cells were incubated with EV71 (MOI = 10) at 4°C for 0.5 h (attachment assay) or incubated at 4°C for 0.5 h followed by 2h of incubation at 37°C (internalization assay). Cells were then washed extensively with ice-cold PBS. Total RNA was extracted, and viral RNA was determined by qPCR. Primers used for qPCR are as follows: VP1-F: AAGGTTCCAGCACTCCAAGC; VP1-R: TCTCCAACTAATCCCGCCC; GAPDH-F: CTCTGCTCCTCCTGTTCGAC; and GAPDH-R: TTAAAAGCAGCCCTGGTGAC.

Immunoblotting and co-immunoprecipitation

Immunoblotting was carried out as previously described (27). Phos-tag gels contained 50 µM Phosbind acrylamide and 100 µM $MnCl_2$. Before transferring, phos-tag gel was immersed in the transfer buffer containing 10 mM EDTA.

Co-immunoprecipitation was performed as previously described (24). Briefly, 293T cells were transfected with the indicated plasmids (500 ng/well) using a JetPRIME transfection reagent (Illkirch, France) according to the manufacturer's protocol. Twenty-four hours later, the cells were harvested with IP buffer [20 mM Tris–HCl, pH 8.0, 137 mM NaCl, 1% Nonidet P-40 (NP-40), and 2 mM EDTA] supplemented with a protease inhibitor cocktail. Cell debris was removed by centrifugation at 12,000 rpm for 10 min at 4°C. The supernatant was incubated with indicated antibodies at 4°C for 2 h on a rotator before they were immunoprecipitated with Dynabeads Protein A/G (Thermo Fisher Scientific) and incubated for another 1 h at 4°C. After washing with wash buffer (0.05% Triton X-100)six times, samples were subjected to SDS-PAGE. The chemiluminescence signals were visualized using ECL Advance reagents (Mishubio, China), and the images were acquired using the FUSION Solo S Imaging System (Vilber, France).

Membrane flotation assay

Membrane flotation was carried out as previously described (19) with the following modification: SK-N-SH cells were infected with EV71 at MOI = 5 and uninfected SK-N-SH cells were used as a control group. After cells were homogenized and treated with 0.05% ice-cold NP-40, the pellets were overlaid to Optiprep gradient and centrifuged with CS150 NX Micro Ultracentrifuge (Eppendorf Himac Technologies) using a S52ST swinging bucket rotor at 45,000 rpm for 4 h at 4°C. After centrifugation, fractions were collected from the top, and proteins were concentrated by TCA (trichloroacetic acid) precipitation and separated by SDS-PAGE for immunoblotting.

Confocal microscopy

Cells seeded on poly-D-lysine-coated glass coverslips were fixed and permeabilized with ice-cold methanol for 20 min. After blocking with 10% FBS for 1 h, the cells were incubated with indicated primary antibodies for 1 h, followed by secondary antibody detection. Coverslips were mounted with Prolong Glass Antifade Mountant (Thermo Fisher Scientific). For phalloidin staining, cells were fixed with 3.7% formaldehyde and permeabilized with 0.1% Triton X-100. FITC-phalloidin was diluted at 1:200. PI4P staining of intracellular membranes was performed exactly as described (39). Images were taken with an FV3000 laser scanning confocal microscope (Olympus, Japan) with sequential scanning mode. PI4P fluorescence intensity was determined from multiple random fields using Fiji software.

Transmission electron microscopy

Control or NAT6 KO cells stably expressing T7 RNA polymerase were seeded in a 6 cm cell culture dish and transfected with pTM1 (2A–3D) to allow EV71 nonstructural proteins expression under the T7 promoter. Thirty-six hours later, cells were harvested for immunoblotting or prepared for TEM. For TEM, cell pellets were fixed with Gluta fixing solution (Solarbio, 2.5% glutaraldehyde solution in 0.2 M phosphate buffer, pH 7.0) at 4°C. Samples were post-fixed in 1% osmium tetroxide, dehydrated in a graded ethanol series, and embedded in Epon. Ultra-thin sections were collected onto copper grids and post-stained with uranyl acetate and lead citrate. The sections were viewed on a Talos L120C transmission electron microscope (ThermoFisher Scientific). The number and size of intracellular vesicles were calculated with Fiji software.

Protein stability assay

To test ACBD3 stability, 293T cells transfected with NAT6 and ACBD3, or SK-N-SH cells stably expressing NAT6 were treated with 100 or 125 µM CHX. Cells were then harvested at indicated time points and subjected to immunoblotting. To test the protein degradation pathways, control or NAT6 KO cells were mock treated or treated with 10 µM MG132 or 10 nM BafA1 for 24 h before samples were collected and immunoblotted.

Statistical analysis

All experiments were performed in triplicates, and data are expressed as means ± standard deviations. Statistical analysis was performed with GraphPad Prism 8.0.1 using unpaired two-tailed Student's *t*-test. ns, not significant; $P > 0.05$; *$P < 0.05$; **$P < 0.01$; and ***$P < 0.001$.

ACKNOWLEDGMENTS

This work was supported by the National Natural Science Foundation of China (82272309) and the Basic and Clinical Medicine Collaboration Project of Xi'an Jiaotong University (YXJLRH20022019).

AUTHOR AFFILIATIONS

[1]Department of Pathogen Biology and Immunology, Xi'an Jiaotong University Health Science Center, Xi'an, China
[2]Department of Gynecology and Obstetrics, The First Affiliated Hospital of Xi'an Jiaotong University, Xi'an, China
[3]Department of Infectious Diseases, The First Affiliated Hospital of Xi'an Jiaotong University, Xi'an, China

AUTHOR ORCIDs

Hang Yang http://orcid.org/0000-0001-7374-0702
Hongliang Wang http://orcid.org/0000-0002-3304-2683

FUNDING

Funder	Grant(s)	Author(s)
MOST | National Natural Science Foundation of China (NSFC)	82272309	Hongliang Wang
Basic and Clinical Medicine Collaboration Project of Xi'an Jiaotong University	YXJLRH20022019	Hongliang Wang

AUTHOR CONTRIBUTIONS

Hang Yang, Formal analysis, Investigation | Tingting Fan, Investigation, Methodology | Meng Xun, Supervision, Validation | Bo Wu, Methodology, Validation | Shangrui Guo, Methodology, Validation, Visualization | Xinyu Li, Validation, Writing – original draft | Xiaohui Zhao, Investigation | Haoyan Yao, Formal analysis, Writing – original draft | Hongliang Wang, Conceptualization, Funding acquisition, Supervision, Writing – original draft, Writing – review and editing

REFERENCES

1. Baggen J, Thibaut HJ, Strating JRPM, van Kuppeveld FJM. 2018. The life cycle of non-polio enteroviruses and how to target it. Nat Rev Microbiol 16:368–381. https://doi.org/10.1038/s41579-018-0022-3
2. Solomon T, Lewthwaite P, Perera D, Cardosa MJ, McMinn P, Ooi MH. 2010. Virology, epidemiology, pathogenesis, and control of enterovirus 71. Lancet Infect Dis 10:778–790. https://doi.org/10.1016/S1473-3099(10)70194-8
3. Rao CD. 2021. Enteroviruses in gastrointestinal diseases. Rev Med Virol 31:1–12. https://doi.org/10.1002/rmv.2148
4. Yamayoshi S, Yamashita Y, Li J, Hanagata N, Minowa T, Takemura T, Koike S. 2009. Scavenger receptor B2 is a cellular receptor for enterovirus 71. Nat Med 15:798–801. https://doi.org/10.1038/nm.1992
5. Hussain KM, Leong KLJ, Ng M-L, Chu JJH. 2011. The essential role of clathrin-mediated endocytosis in the infectious entry of human enterovirus 71. J Biol Chem 286:309–321. https://doi.org/10.1074/jbc.M110.168468
6. Yuan J, Shen L, Wu J, Zou X, Gu J, Chen J, Mao L. 2018. Enterovirus A71 proteins: structure and function. Front Microbiol 9:286. https://doi.org/10.3389/fmicb.2018.00286
7. Wang H, Li Y. 2019. Recent progress on functional genomics research of enterovirus 71. Virol Sin 34:9–21. https://doi.org/10.1007/s12250-018-0071-9
8. Guo H, Li Y, Liu G, Jiang Y, Shen S, Bi R, Huang H, Cheng T, Wang C, Wei W. 2019. A second open reading frame in human enterovirus determines viral replication in intestinal epithelial cells. Nat Commun 10:4066. https://doi.org/10.1038/s41467-019-12040-9
9. Lulla V, Dinan AM, Hosmillo M, Chaudhry Y, Sherry L, Irigoyen N, Nayak KM, Stonehouse NJ, Zilbauer M, Goodfellow I, Firth AE. 2019. An upstream protein-coding region in enteroviruses modulates virus infection in gut epithelial cells. Nat Microbiol 4:280–292. https://doi.org/10.1038/s41564-018-0297-1
10. Miller S, Krijnse-Locker J. 2008. Modification of intracellular membrane structures for virus replication. Nat Rev Microbiol 6:363–374. https://doi.org/10.1038/nrmicro1890
11. Wolff G, Melia CE, Snijder EJ, Bárcena M. 2020. Double-membrane vesicles as platforms for viral replication. Trends Microbiol 28:1022–1033. https://doi.org/10.1016/j.tim.2020.05.009
12. Li X, Wang M, Cheng A, Wen X, Ou X, Mao S, Gao Q, Sun D, Jia R, Yang Q, Wu Y, Zhu D, Zhao X, Chen S, Liu M, Zhang S, Liu Y, Yu Y, Zhang L, Tian B, Pan L, Chen X. 2020. Enterovirus replication organelles and inhibitors of their formation. Front Microbiol 11:1817. https://doi.org/10.3389/fmicb.2020.01817
13. Melia CE, Peddie CJ, de Jong AWM, Snijder EJ, Collinson LM, Koster AJ, van der Schaar HM, van Kuppeveld FJM, Bárcena M. 2019. Origins of enterovirus replication organelles established by whole-cell electron microscopy. mBio 10:e00951-19. https://doi.org/10.1128/mBio.00951-19
14. Limpens R, van der Schaar HM, Kumar D, Koster AJ, Snijder EJ, van Kuppeveld FJM, Bárcena M. 2011. The transformation of enterovirus replication structures: a three-dimensional study of single- and double-membrane compartments. mBio 2:e00166-11. https://doi.org/10.1128/mBio.00166-11
15. Belov GA, Nair V, Hansen BT, Hoyt FH, Fischer ER, Ehrenfeld E. 2012. Complex dynamic development of poliovirus membranous replication complexes. J Virol 86:302–312. https://doi.org/10.1128/JVI.05937-11
16. Hsu N-Y, Ilnytska O, Belov G, Santiana M, Chen Y-H, Takvorian PM, Pau C, van der Schaar H, Kaushik-Basu N, Balla T, Cameron CE, Ehrenfeld E, van Kuppeveld FJM, Altan-Bonnet N. 2010. Viral reorganization of the secretory pathway generates distinct organelles for RNA replication. Cell 141:799–811. https://doi.org/10.1016/j.cell.2010.03.050
17. Balla A, Balla T. 2006. Phosphatidylinositol 4-kinases: old enzymes with emerging functions. Trends Cell Biol 16:351–361. https://doi.org/10.1016/j.tcb.2006.05.003

18. Roulin PS, Lötzerich M, Torta F, Tanner LB, van Kuppeveld FJM, Wenk MR, Greber UF. 2014. Rhinovirus uses a phosphatidylinositol 4-phosphate/cholesterol counter-current for the formation of replication compartments at the ER-Golgi interface. Cell Host Microbe 16:677–690. https://doi.org/10.1016/j.chom.2014.10.003
19. Wang H, Perry JW, Lauring AS, Neddermann P, De Francesco R, Tai AW. 2014. Oxysterol-binding protein is a phosphatidylinositol 4-kinase effector required for HCV replication membrane integrity and cholesterol trafficking. Gastroenterology 146:1373–1385. https://doi.org/10.1053/j.gastro.2014.02.002
20. Sasaki J, Ishikawa K, Arita M, Taniguchi K. 2012. ACBD3-mediated recruitment of PI4KB to picornavirus RNA replication sites. EMBO J 31:754–766. https://doi.org/10.1038/emboj.2011.429
21. Lyoo H, van der Schaar HM, Dorobantu CM, Rabouw HH, Strating J, van Kuppeveld FJM. 2019. Acbd3 is an essential pan-enterovirus host factor that mediates the interaction between viral 3A protein and cellular protein PI4KB. mBio 10:e02742-18. https://doi.org/10.1128/mBio.02742-18
22. Diep J, Ooi YS, Wilkinson AW, Peters CE, Foy E, Johnson JR, Zengel J, Ding S, Weng K-F, Laufman O, Jang G, Xu J, Young T, Verschueren E, Kobluk KJ, Elias JE, Sarnow P, Greenberg HB, Hüttenhain R, Nagamine CM, Andino R, Krogan NJ, Gozani O, Carette JE. 2019. Enterovirus pathogenesis requires the host methyltransferase SETD3. Nat Microbiol 4:2523–2537. https://doi.org/10.1038/s41564-019-0551-1
23. Kung Y-A, Chiang H-J, Li M-L, Gong Y-N, Chiu H-P, Hung C-T, Huang P-N, Huang S-Y, Wang P-Y, Hsu T-A, Brewer G, Shih S-R, Marie Hardwick J, Griffin DE. 2022. Acyl-Coenzyme a synthetase long-chain family member 4 is involved in viral replication organelle formation and facilitates virus replication via ferroptosis. mBio 13:e0271721. https://doi.org/10.1128/mbio.02717-21
24. Zhao X, Yuan H, Yang H, Liu Y, Xun M, Li X, Fan T, Wu B, Guo S, Wang H. 2022. N-acetyltransferase 8 promotes viral replication by increasing the stability of enterovirus 71 nonstructural proteins. J Virol 96:e0011922. https://doi.org/10.1128/jvi.00119-22
25. Baggen J, Thibaut HJ, Staring J, Jae LT, Liu Y, Guo H, Slager JJ, de Bruin JW, van Vliet ALW, Blomen VA, Overduin P, Sheng J, de Haan CAM, de Vries E, Meijer A, Rossmann MG, Brummelkamp TR, van Kuppeveld FJM. 2016. Enterovirus D68 receptor requirements unveiled by haploid genetics. Proc Natl Acad Sci U S A 113:1399–1404. https://doi.org/10.1073/pnas.1524498113
26. Aksnes H, Ree R, Arnesen T. 2019. Co-translational, post-translational, and non-catalytic roles of N-terminal acetyltransferases. Mol Cell 73:1097–1114. https://doi.org/10.1016/j.molcel.2019.02.007
27. Yang H, Zhao X, Xun M, Ma C, Wang H. 2021. Reverse genetic approaches for the generation of full length and subgenomic replicon of EV71 virus. Front Microbiol 12:665879. https://doi.org/10.3389/fmicb.2021.665879
28. Drazic A, Aksnes H, Marie M, Boczkowska M, Varland S, Timmerman E, Foyn H, Glomnes N, Rebowski G, Impens F, Gevaert K, Dominguez R, Arnesen T. 2018. NAA80 is actin's N-terminal acetyltransferase and regulates cytoskeleton assembly and cell motility. Proc Natl Acad Sci U S A 115:4399–4404. https://doi.org/10.1073/pnas.1718336115
29. Ree R, Kind L, Kaziales A, Varland S, Dai M, Richter K, Drazic A, Arnesen T. 2020. PFN2 and NAA80 cooperate to efficiently acetylate the N-terminus of actin. J Biol Chem 295:16713–16731. https://doi.org/10.1074/jbc.RA120.015468
30. Ilnytska O, Santiana M, Hsu NY, Du WL, Chen YH, Viktorova EG, Belov G, Brinker A, Storch J, Moore C, Dixon JL, Altan-Bonnet N. 2013. Enteroviruses harness the cellular Endocytic machinery to Remodel the host cell cholesterol landscape for effective viral replication. Cell Host & Microbe 14:281–293. https://doi.org/10.1016/j.chom.2013.08.002
31. van der Schaar HM, Dorobantu CM, Albulescu L, Strating JRPM, van Kuppeveld FJM. 2016. Fat(al) attraction: picornaviruses usurp lipid transfer at membrane contact sites to create replication organelles. Trends Microbiol. 24:535–546. https://doi.org/10.1016/j.tim.2016.02.017
32. Saxena V, Lai C-K, Chao T-C, Jeng K-S, Lai MMC. 2012. Annexin A2 is involved in the formation of hepatitis C virus replication complex on the lipid raft. J Virol 86:4139–4150. https://doi.org/10.1128/JVI.06327-11
33. Beigl TB, Hellesvik M, Saraste J, Arnesen T, Aksnes H. 2020. N-terminal acetylation of actin by NAA80 is essential for structural integrity of the Golgi apparatus. Exp Cell Res 390:111961. https://doi.org/10.1016/j.yexcr.2020.111961
34. Chen YH, Du W, Hagemeijer MC, Takvorian PM, Pau C, Cali A, Brantner CA, Stempinski ES, Connelly PS, Ma HC, Jiang P, Wimmer E, Altan-Bonnet G, Altan-Bonnet N. 2015. Phosphatidylserine vesicles enable efficient en bloc transmission of enteroviruses. Cell 160:619–630. https://doi.org/10.1016/j.cell.2015.01.032
35. Robinson SM, Tsueng G, Sin J, Mangale V, Rahawi S, McIntyre LL, Williams W, Kha N, Cruz C, Hancock BM, Nguyen DP, Sayen MR, Hilton BJ, Doran KS, Segall AM, Wolkowicz R, Cornell CT, Whitton JL, Gottlieb RA, Feuer R. 2014. Coxsackievirus B exits the host cell in shed microvesicles displaying autophagosomal markers. PLoS Pathog 10:e1004045. https://doi.org/10.1371/journal.ppat.1004045
36. Tai AW, Salloum S. 2011. The role of the phosphatidylinositol 4-kinase PI4Ka in hepatitis C virus-induced host membrane rearrangement. PLoS One 6:e26300. https://doi.org/10.1371/journal.pone.0026300
37. Cerikan B, Goellner S, Neufeldt CJ, Haselmann U, Mulder K, Chatel-Chaix L, Cortese M, Bartenschlager R. 2020. A non-replicative role of the 3' terminal sequence of the dengue virus genome in membranous replication organelle formation. Cell Rep 32:107859. https://doi.org/10.1016/j.celrep.2020.107859
38. Minogue S, Waugh MG. 2012. The phosphatidylinositol 4-Kinases: don't call it a comeback. Subcell Biochem 58:1–24. https://doi.org/10.1007/978-94-007-3012-0_1
39. Hammond GRV, Schiavo G, Irvine RF. 2009. Immunocytochemical techniques reveal multiple, distinct cellular pools of Ptdins4P and Ptdins(4,5)P(2). Biochem J 422:23–35. https://doi.org/10.1042/BJ20090428
40. Sasaki J, Ishikawa K, Arita M, Taniguchi K. 2012. ACBD3-mediated recruitment of PI4KB to picornavirus RNA replication sites. EMBO J 31:754–766. https://doi.org/10.1038/emboj.2011.429
41. Yue X, Qian Y, Zhu L, Gim B, Bao M, Jia J, Jing S, Wang Y, Tan C, Bottanelli F, Ziltener P, Choi S, Hao P, Lee I. 2021. ACBD3 modulates KDEL receptor interaction with PKA for its trafficking via tubulovesicular carrier. BMC Biol 19:194. https://doi.org/10.1186/s12915-021-01137-7
42. Drazic A, Aksnes H, Marie M, Boczkowska M, Varland S, Timmerman E, Foyn H, Glomnes N, Rebowski G, Impens F, Gevaert K, Dominguez R, Arnesen T. 2018. NAA80 is actin's N-terminal acetyltransferase and regulates cytoskeleton assembly and cell motility. Proc Natl Acad Sci U S A 115:4399–4404. https://doi.org/10.1073/pnas.1718336115
43. Kulkarni-Gosavi P, Makhoul C, Gleeson PA. 2019. Form and function of the Golgi apparatus: Scaffolds, cytoskeleton and signalling. FEBS Lett 593:2289–2305. https://doi.org/10.1002/1873-3468.13567
44. Lázaro-Diéguez F, Jiménez N, Barth H, Koster AJ, Renau-Piqueras J, Llopis JL, Burger KNJ, Egea G. 2006. Actin filaments are involved in the maintenance of Golgi cisternae morphology and intra-Golgi pH. Cell Motil Cytoskeleton 63:778–791. https://doi.org/10.1002/cm.20161
45. Song HP, Zhang J, He W, Wang P, Wang FJ. 2019. Activation of cofilin increases intestinal permeability depolymerization of F-actin during hypoxia. Front Physiol 10. https://doi.org/10.3389/fphys.2019.01455
46. Lázaro-Diéguez F, Aguado C, Mato E, Sánchez-Ruíz Y, Esteban I, Alberch J, Knecht E, Egea G. 2008. Dynamics of an F-actin aggresome generated by the actin-stabilizing toxin jasplakinolide. J Cell Sci 121:1415–1425. https://doi.org/10.1242/jcs.017665
47. Zhang X, Wang Y. 2020. Nonredundant roles of GRASP55 and GRASP65 in the Golgi apparatus and beyond. Trends Biochem Sci 45:1065–1079. https://doi.org/10.1016/j.tibs.2020.08.001
48. Wessels E, Duijsings D, Lanke KHW, van Dooren SHJ, Jackson CL, Melchers WJG, van Kuppeveld FJM. 2006. Effects of picornavirus 3A proteins on protein transport and GBF1-dependent COP-I recruitment. J Virol 80:11852–11860. https://doi.org/10.1128/JVI.01225-06
49. Goris M, Magin RS, Foyn H, Myklebust LM, Varland S, Ree R, Drazic A, Bhambra P, Støve SI, Baumann M, Haug BE, Marmorstein R, Arnesen T. 2018. Structural determinants and cellular environment define processed actin as the sole substrate of the N-terminal acetyltransferase NAA80. Proc Natl Acad Sci U S A 115:4405–4410. https://doi.org/10.1073/pnas.1719251115
50. Yue XH, Bao MJ, Christiano R, Li SY, Mei J, Zhu LH, Mao FF, Yue Q, Zhang PP, Jing SY, Rothman JE, Qian Y, Lee I. 2017. ACBD3 functions as a scaffold to organize the Golgi stacking proteins and a Rab33B-GAP. FEBS Lett 591:2793–2802. https://doi.org/10.1002/1873-3468.12780
51. Chalupska D, Różycki B, Humpolickova J, Faltova L, Klima M, Boura E. 2019. Phosphatidylinositol 4-kinase IIIβ (Pi4KB) forms highly flexible

heterocomplexes that include ACBD3, 14-3-3, and Rab11 proteins. Sci Rep 9:567. https://doi.org/10.1038/s41598-018-37158-6
52. Tang D, Zhang X, Huang S, Yuan H, Li J, Wang Y, Glick BS. 2016. Mena-GRASP65 interaction couples actin polymerization to Golgi ribbon linking. Mol Biol Cell 27:137–152. https://doi.org/10.1091/mbc.E15-09-0650
53. Kruppa AJ, Kendrick-Jones J, Buss F. 2016. Myosins, actin and autophagy. Traffic 17:878–890. https://doi.org/10.1111/tra.12410
54. Zhang C, Li Y, Li J. 2020. Dysregulated autophagy contributes to the pathogenesis of enterovirus A71 infection. Cell Biosci 10:142. https://doi.org/10.1186/s13578-020-00503-2
55. Guo S, Xun M, Fan T, Li X, Yao H, Li X, Wu B, Yang H, Ma C, Wang H. 2023. Construction of coxsackievirus B5 viruses with luciferase reporters and their applications *in vitro* and *in vivo*. Virol Sin 38:549–558. https://doi.org/10.1016/j.virs.2023.05.010
56. Li X, Yang E, Li X, Fan T, Guo S, Yang H, Wu B, Wang H. 2023. MAVS-based reporter systems for real-time imaging of EV71 infection and antiviral testing. Viruses 15:1064. https://doi.org/10.3390/v15051064
57. Wang H, Tai AW. 2019. Nir2 is an effector of VAPs necessary for efficient hepatitis C virus replication and phosphatidylinositol 4-phosphate enrichment at the viral replication organelle. J Virol 93:e00742-19. https://doi.org/10.1128/JVI.00742-19